JACS
JOURNAL OF THE AMERICAN CHEMICAL SOCIETY

pubs.acs.org/JACS

Article

In Vivo Photocontrol of Microtubule Dynamics and Integrity, Migration and Mitosis, by the Potent GFP-Imaging-Compatible Photoswitchable Reagents SBTubA4P and SBTub2M

Li Gao, Joyce C. M. Meiring, Adam Varady, Iris E. Ruider, Constanze Heise, Maximilian Wranik, Cecilia D. Velasco, Jennifer A. Taylor, Beatrice Terni, Tobias Weinert, Jörg Standfuss, Clemens C. Cabernard, Artur Llobet, Michel O. Steinmetz, Andreas R. Bausch, Martin Distel, Julia Thorn-Seshold, Anna Akhmanova, and Oliver Thorn-Seshold*

Cite This: *J. Am. Chem. Soc.* 2022, 144, 5614–5628

Read Online

ACCESS | Metrics & More | Article Recommendations | Supporting Information

ABSTRACT: Photoswitchable reagents are powerful tools for high-precision studies in cell biology. When these reagents are globally administered yet locally photoactivated in two-dimensional (2D) cell cultures, they can exert micron- and millisecond-scale biological control. This gives them great potential for use in biologically more relevant three-dimensional (3D) models and *in vivo*, particularly for studying systems with inherent spatiotemporal complexity, such as the cytoskeleton. However, due to a combination of photoswitch isomerization under typical imaging conditions, metabolic liabilities, and insufficient water solubility at effective concentrations, the *in vivo* potential of photoswitchable reagents addressing cytosolic protein targets remains largely unrealized. Here, we optimized the potency and solubility of metabolically stable, druglike colchicinoid microtubule inhibitors based on the styrylbenzothiazole (SBT) scaffold that are nonresponsive to typical fluorescent protein imaging wavelengths and so enable multichannel imaging studies. We applied these reagents both to 3D organoids and tissue explants and to classic model organisms (zebrafish, clawed frog) in one- and two-protein imaging experiments, in which spatiotemporally localized illuminations allowed them to photocontrol microtubule dynamics, network architecture, and microtubule-dependent processes *in vivo* with cellular precision and second-level resolution. These nanomolar, *in vivo* capable photoswitchable reagents should open up new dimensions for high-precision cytoskeleton research in cargo transport, cell motility, cell division, and development. More broadly, their design can also inspire similarly capable optical reagents for a range of cytosolic protein targets, thus bringing *in vivo* photopharmacology one step closer to general realization.

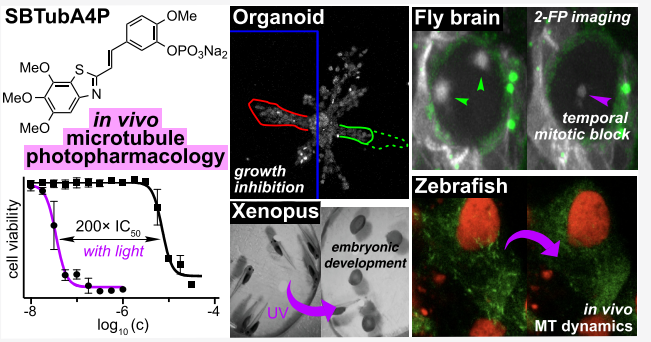

1. INTRODUCTION

Biological methods and instrumentation now allow us to observe cellular structures and dynamics on the micron scale, with dynamics resolved to the scale of milliseconds, in settings from *in vitro* cell culture[1] to *in vivo* (multiorgan) animal models.[2] However, the development of tools to manipulate cellular processes with matching micrometer spatial precision and millisecond temporal precision has lagged far behind, despite its value for research.[3,4]

One biological system with particularly urgent need of such tools is the microtubule (MT) cytoskeleton.[5,6] MTs are giant tubelike noncovalent polymers of α/β-tubulin protein heterodimers that extend throughout the cytosol. They are centrally organized and can be rapidly remodeled to support hundreds of spatiotemporally regulated functions in the life of a cell. The most visible roles of MTs include force generation to maintain and change cell shape and position, and scaffolding the transport of cargos by motor proteins, including chromosomes during cell division. Tools to noninvasively manipulate MT network structure and remodeling dynamics with high spatiotemporal precision have great potential to drive biological research. However, to fulfill this potential, tools must succeed in settings from two-dimensional (2D) cell culture (e.g., cell migration and division) through to *in vivo*, three-dimensional (3D) systems (embryonic development and neuroscience). It is also important that tools be easily transferrable across different models and organisms.[7,8]

Received: January 26, 2022
Published: March 15, 2022

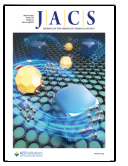

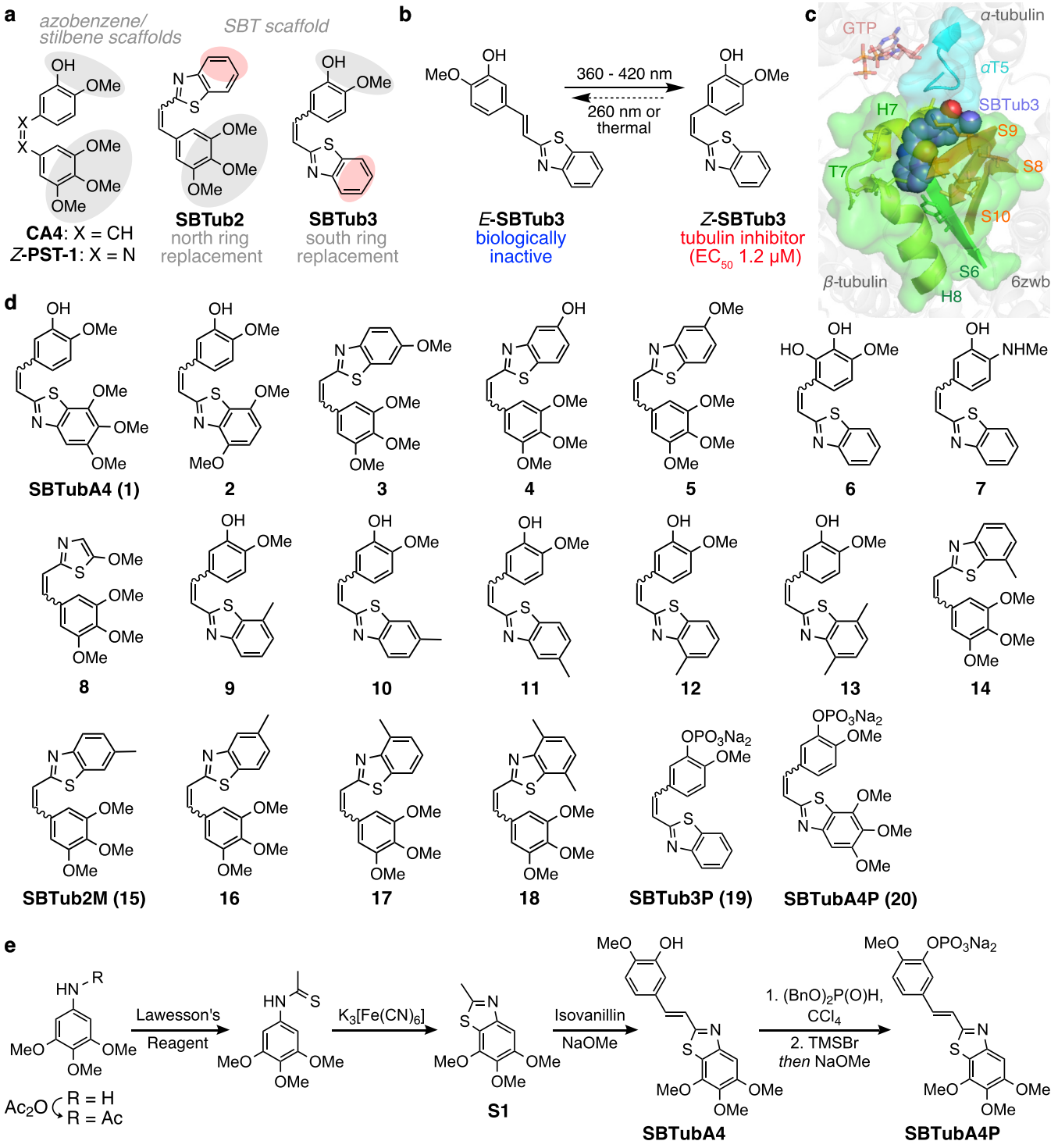

Figure 1. Design and synthesis. (a) The colchicinoid pharmacophore (gray shaded trimethoxyphenyl south ring and isovanillyl north ring) can be applied to various scaffolds, giving photoswitchable azobenzene-based **PST** and SBT-based **SBTub** antimitotics. Previously published **SBTub2/3** lacked key interaction residues (red shaded sites). (b) *Z*-**SBTub3** inhibits tubulin polymerization and MT-dependent processes. (c) X-ray structure of tubulin:*Z*-**SBTub3** complex (carbons as purple spheres). The south ring is buried in β-tubulin (green); only the north ring interacts with α-tubulin at the α-T5 loop (cyan). (d) Evolved SBTub compound library used in this paper. (e) Typical synthesis of SBTubs proceeds by acetanilide sulfurization, Jacobson cyclization, and basic condensation. Phosphate prodrug **SBTubA4P** is further accessed by phosphoester formation and deprotection.

Optogenetics has been extremely successful in patterning ion currents and cell signaling with high spatiotemporal precision. However, until recently, only two optogenetic tools to modulate MT dynamics and network architecture were known: Wittmann's photo-inactivatable MT-polymerizing tool π-EB1,[9] and Slep's photoactivated plus tip recruitment system.[10] Two further optogenetic tools to photocontrol enzymatic severing of MTs have recently appeared as preprints,[11,12] highlighting the interest in methods to photocontrol microtubule dynamics, network organization, and interaction partners.

By comparison, drugs to modulate MT structure and dynamics reliably across all eukaryotes are very well studied,

https://doi.org/10.1021/jacs.2c01020
J. Am. Chem. Soc. 2022, 144, 5614−5628

with their ease of being translated across models and species (no time needed for breeding and validating transgenic lines, optimizing expression systems, etc.) being a strong practical advantage over genetic approaches. Taxanes, epothilones, colchicine analogues, and vinca alkaloids are all used for nonspecific suppression of MT-dependent cellular processes, in settings from single-cell studies through to *in vivo* therapeutic use in humans.

Much effort has been invested to develop light-triggered analogues of these drugs, to improve the spatiotemporal precision with which their MT-inhibiting activity can be applied (toward the scale of μm and ms). Photouncaging approaches have been known for some decades;[13] while more recently, photoisomerization-based drug analogues or "photopharmaceuticals" have been developed, to elegantly avoid many of the drawbacks that limited the *in vivo* use of typical photouncaging methods,[14] such as toxic and/or phototoxic byproducts, requirements for <360 nm wavelengths and high light intensities, slow post-illumination fragmentation, irreversibly photosensitive stock solutions, and non-optical drug release mechanisms (e.g., enzymatic hydrolysis of cages). In the MT field, recent photoswitchable analogues of taxane,[15] epothilone,[16] and colchicinoid[5,17−22] MT inhibitors have all been applied to cellular studies. These photopharmaceuticals have enabled noninvasive, reversible optical control over MT dynamics and MT-associated downstream effects, with cell-specific spatial precision and subsecond-scale temporal precision, and have been brought to bear on research in embryology,[23] neuroscience,[24] and cytoskeleton.[5]

However, the typical photoswitch scaffolds introduce problems particularly for *in vivo* application, three of which this paper will focus on: (1) **Metabolic stability**: azobenzenes, particularly as their *Z*-isomers, can be reductively degraded by cellular glutathione (GSH), although the substituent-dependency of this degradation has not yet been elucidated.[25−27] This degradation reduces reagent photoswitchability as well as potency, and on timescales typical for *in vivo* studies (>hours) the degradation byproducts are likely to give off-target effects, particularly in metabolically active later-stage animals (tested below, and also discussed elsewhere[18]). (2) **Orthogonal photocontrol and imaging**: under the high intensities of focussed lasers in microscopy, azobenzenes and hemithioindigos are isomerized by excitation of the typical fluorescent proteins or labels imaged in biological studies (GFP/fluorescein at 490 nm, YFP at 514 nm; some also isomerize with RFP/rhodamine imaging at 561 nm).[18,28] Typically this leaves only the 647 nm laser channel available for orthogonal imaging during photoswitching, yet this laser typically only addresses small-molecule probes. These scaffolds' inability to allow multichannel protein imaging during photocontrol is particularly problematic for *in vivo* research that extensively relies on two- or three-channel imaging with fluorescent protein fusions to resolve processes with biological specificity. (3) **Practical applicability**: *in vivo* studies must ensure sufficient delivery of photopharmaceuticals to target tissues without organic cosolvents, which are less tolerated by embryos than they are in cell culture. This requires either high-potency compounds or effective solubilizing strategies: neither of which are often seen with typically hydrophobic photoswitchable drug analogues. A separate concern is to minimize the illumination needed to photoswitch an effective amount of reagent (another problem that is more urgent for *in vivo* than cellular studies). Photoswitch performance at optimal but unavailable wavelengths (e.g., 260−380 nm) is irrelevant for this: tuning the scaffold's photoresponse at the laser wavelength actually used in biological studies[18] is required, to reach both high efficiency of isomerization $E(\lambda)$[5] as well as a high photostationary state (PSS).

Novel photoswitches addressing these issues are recently gaining attention to expand the biological scope of photopharmacology.[29−31] To tackle them in the context of microtubule photocontrol, we previously introduced styrylbenzothiazoles **SBTub2/3** (Figure 1a) as highly metabolically stable, fully GFP/YFP/RFP-orthogonal photoswitchable tubulin inhibitors (Figure 1b,c), with excellent photoresponse to the 405 nm laser line that is standard in confocal microscopy. **SBTub3** could photocontrol MT dynamics, organization, and MT-dependent processes in live cells with reversible temporal patterning, and with cellular and even subcellular spatial precision.[18]

The metabolic stability and imaging-orthogonal photocontrol of **SBTub3** were excellent features toward *in vivo* use, but practical limitations remained, which we determined to address in this study. Primarily, while their parent colchicinoid inhibitor combretastatin A-4 (**CA4**) has ca. 20 nM cellular potency, the slightly larger *Z*-**SBTub2/3** gave only micromolar bioactivity (though note that the **CA4**-isosteric azobenzene analogue *Z*-**PST-1** has only ca. 500 nM potency; Figure 1a). The lower the potency, the more compound and the more cosolvent are needed, which we found blocked animal model applications of both **SBTub2/3** and **PST-1** (see below). Thus, we prioritized a structure−activity relationship (SAR) study to improve the potency of **SBTub**s (Figure 1d). Second, the **SBTub**s are hydrophobic, so we prioritized fully water-soluble prodrugs for *in vivo* use without cosolvents. Third, while the SBT scaffold is essentially a unidirectional ($E \rightarrow Z$) photoswitch in the biological range because its isomers' absorption bands overlap, we were curious if tautomerizable electron-donating substituents could accelerate its spontaneous thermal $Z \rightarrow E$ relaxation, as they do for azobenzenes, toward deriving SBT-based photopharmaceuticals with appreciable rates of spontaneous "bioactivity switch-off".[28]

Our goal was then to test whether suitably potent and soluble SBT derivatives could be used for photocontrol not only in cell culture settings where many photoswitches succeed, but over a range of *in vivo* multi-organ animal models, with temporally specific and cell-precise *in situ* photoswitching after systemic administration: settings in which no other photoswitchable reagents have so far succeeded. We now report the development of these potent, soluble, metabolically stable, GFP-orthogonal SBT-based photopharmaceuticals, and characterize the optimal ligands **SBTubA4** and with tubulin:SBT X-ray crystal structures. We then showcase the unprecedented success of the fully water-soluble prodrug **SBTubA4P** in allowing systemic administration but local photoactivations to achieve (i) spatiotemporally specific control over MT dynamics in cell culture, (ii) long-term spatially specific control over development and migration in 3D organoid culture, (iii) short-term temporally resolved photocontrol of neural development in fly brain explant, (iv) photocontrol of embryonic development in the clawed frog, and (v) temporally reversible photocontrol of microtubule dynamics in zebrafish.

2. RESULTS

2.1. Cellular Structure−Activity Optimization of SBTubs. For a colchicinoid **SBTub** to be cellularly effective, its *Z*-isomer should bind tubulin,[5,32] halting cell proliferation and inducing apoptosis;[33] while the *E*-isomer should have

https://doi.org/10.1021/jacs.2c01020
J. Am. Chem. Soc. 2022, 144, 5614−5628

negligible tubulin binding and no other significant toxicity mechanisms over a wide concentration range where the *Z*-isomer is bioactive, resulting in a high lit/dark bioactivity ratio ("photoswitchability of bioactivity").[18] Thus, we performed cellular structure–activity optimization by comparing the proliferation of cells treated with **SBTubs** (Table 1 and Figure S5) under *in situ* pulsed illuminations with near-UV light ("lit": mostly-*Z*-isomer; aim: nanomolar EC_{50}), to their proliferation without illumination ("dark": all-*E*-isomer; aim: no antiproliferative effects at concentrations of up to 100 times the lit EC_{50}).

Table 1. Cytotoxicity EC_{50} Values [mostly-*Z* lit ($h\nu$ 360–450 nm), all-*E* dark] and Dark/Lit EC_{50} Ratio; and Standard Photoactivation Working Concentration $[I]_{WC}$ [all in HeLa cell line; na: analysis not applicable (see Supporting Information)]

	EC_{50} (μM)		EC_{50} ratio	$[I]_{WC}$
compound	$h\nu$	dark	dark/lit	(μM)
SBTub2	1.4	>25	>18	6.0
SBTub3	1.2	>25	>21	3.2
SBTubA4	0.12	3.8	31	0.21
2	0.52	>100	>190	1.6
3	0.20	15	75	0.65
4	0.67	9.3	14	1.5
5	1.4	18	13	3.2
6	23	27	na	na
7	2.6	>35	>13	na
8	1.2	>100	>83	3.0
9	1.0	48	48	2.6
10	3.0	>100	>33	10
11	1.7	>100	>58	4.3
12	0.77	64	83	1.6
13	0.42	8.8	21	1.8
14	1.0	>15	>14	2.7
SBTub2M	0.035	7.0	**200**	**0.06**
16	0.52	48	92	1.1
17	0.23	40	174	0.65
18	3.0	>15	>5	10
SBTub3P	3.4	>20	>5	7.5
SBTubA4P	0.052	0.45	8.7	**0.10**

We furthermore introduce a single metric, the "typically useful working concentration for cell culture" $[I]_{WC}$, by which to rank photopharmaceuticals for their practical utility (Table 1) and so guide optimization. $[I]_{WC}$ is derived by examining the dose–response curves (Figures 2a and S5) to find the lowest concentration at which illuminated cells experience strong inhibition while nonilluminated cells experience insignificant inhibition. We systematically define $[I]_{WC}$ as either the lowest concentration where the lit efficacy reaches >80% of its plateau, or the highest concentration where treatment in the dark causes <10% difference of biological effect compared to the untreated control: whichever is the lower (Figure 2a). Szymanski has previously proposed an alternative working concentration metric $[I]_{opt}$, which emphasizes maximal illuminated efficacy, and is based on idealized dose–response curves with high Hill coefficients[4] that are rarely obtained in practice. Our empirical $[I]_{WC}$ instead emphasizes our experience that baseline/background inhibition of biological systems must be minimal for photopharmaceutical control to be biologically useful. For example, even if IC_{50} values are well separated, $[I]_{WC}$ values are undefined if background bioactivity is too strong for the reagent

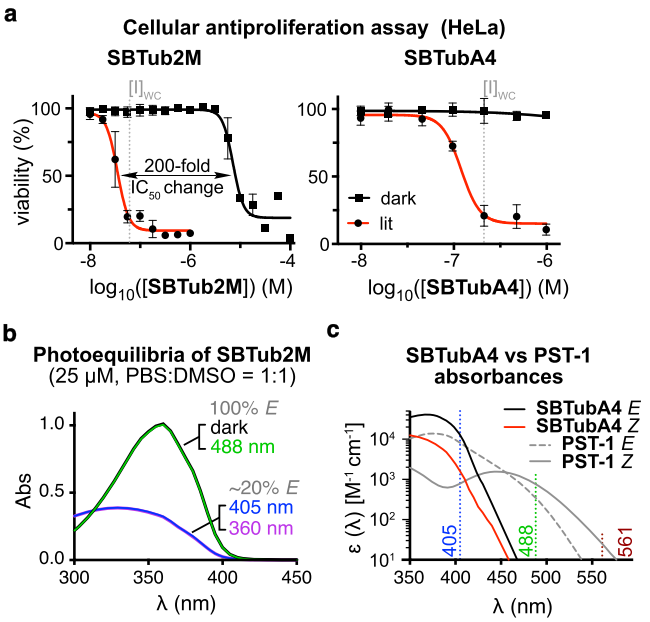

Figure 2. (a) Leads **SBTub2M** and **SBTubA4** have highly nonlinear dose–response profiles, high lit/dark ratio of bioactivity, and mid-nanomolar $[I]_{WC}$ values. (b, c) Photocharacterization: (b) **SBTub2M** is not isomerized from its all-*E* dark state by 488 nm illumination, but is photoswitched to majority-*Z* lit states by UV/violet light (78% *Z* at 405 nm by NMR; 1:1 phosphate-buffered saline/dimethylsulfoxide, PBS:DMSO). (c) Comparison of absorbance spectra of **SBTubA4** and azobenzene **PST-1** illustrates the SBT's ideal match to 405 nm photoactivation, combining stronger 405 nm absorption, with sharper absorption cutoff above 405 nm, which makes it orthogonal to GFP (488 nm), YFP (514 nm), and RFP (561 nm) imaging.

Our first priority for *in vivo* use was to increase *Z*-**SBTub** potency. We first tested whether restoring the methoxy groups of the **CA4** pharmacophore would increase potency despite the extra size, with **SBTubA4** (**1**). This, like most **SBTubs**, was synthesized in a short sequence (Figure 1e) via basic aldol condensation of the derivatized 2-methylbenzothiazole with the corresponding benzaldehyde, with the 2-methylbenzothiazole being obtained *via* Jacobson cyclization[34] of the thioacetanilide using potassium ferricyanide (exceptions were *para*-aniline **7** which was obtained by Horner-Wadsworth-Emmons olefination; and **9** and **11** where 2,5-/2,7-dimethylbenzothiazoles were synthesized by Ullmann-type coupling according to Ma;[35] see the Supporting Information).

SBTubA4 was an early hit, with a ca. 10-fold more potent *Z*-isomer than the previous best **SBTub3** and with an excellent dark/lit ratio of 30 (Figure 2a). We then tested if the *Z*-**SBTubs** obey similar structure–activity relationships (SAR) as known for **CA4**. First, we rearranged the methoxy groups in **2**, reducing the *Z*-potency, which matched literature expectations[36] as the middle methoxy group on the south ring otherwise accepts a hydrogen bond from β-Cys239. We also flipped the SBT scaffold orientation in analogues **3**–**5**. This was not convenient for installing the hydroxy/methoxy north ring substituent pair, so in **3** and **4** we retained only one of these groups and the compounds suffered a predictable[36] though a small loss of potency. The 7-fold potency loss when moving the methoxy group from the

https://doi.org/10.1021/jacs.2c01020
J. Am. Chem. Soc. 2022, 144, 5614–5628

space-filling 6-position to the 5-position which is best occupied by a small polar substituent (compound **5**) was striking and expected. We concluded that indeed *Z*-**SBTub**s obey similar SAR as **CA4**, which could guide further development.

At this stage, we wished to test if common strategies to accelerate thermal $Z \rightarrow E$ relaxation and redshift spectral response in azobenzenes could also be applied to **SBTubs**. We created close steric matches of bioactive **SBTub3** but with tautomerizable *ortho*-catechol **6** and *para*-amino **7** groups. Since *o*-hydroxy derivatives of **CA4** have entered clinical trials,[36] we were surprised that **6** gave negligible potency under lit (and dark) conditions; however, **7** retained similar light-specific bioactivity as its isostere **SBTub3** (see Section 2.2).

Continuing potency optimization, we also tested whether retaining the **CA4** methoxy groups on a reduced-size photoswitch would be beneficial. We created styrylthiazole (ST) **8** which can be considered as a near-perfect isostere of **CA4**/**PST-1** minus the small polar hydroxyl group, or as a shrunken analogue of **3**. As far as we know, STs have never been used in photopharmacology before. We considered them interesting to the field as we expected them to retain the metabolic stability and GFP orthogonality of SBT, while additionally being isosteric to the better-known azobenzene: which offers attractive possibilities for adapting known azobenzenes (against other targets) into potentially biologically more applicable ST-based photopharmaceuticals. **8** was accessed by closing the thiazole, starting from a methyl cinnamoylglycinate (see the Supporting Information). Pleasingly, **8** gave strong *Z*-specific cellular bioactivity with ca. 100-fold photoswitchability, although its 10-fold loss of potency compared to **1** suggested that for the colchicine site, we should explore **SBTubs** intermediate in size between **SBTub3** and **1**.

Therefore, for potency optimization, we tested both adding methyl groups to **SBTub3** and "walking" them around the scaffold south ring (**9**−**13**); and also deleting the north ring hydroxy/methoxy substituent pair from **1** and replacing them with smaller methyls (**14**−**18**). Since SBT *Z*-isomers orient their sulfur toward the inner face of the molecule,[18] we did not rely on rotations around the alkene—benzothiazole single bond to "reflect" substituents into similar positions (e.g., **9** vs **12**, or **10** vs **11**).

South ring derivatives **9**−**13** did not approach the potency of **1**−**5**, although **10**−**11** still have excellent performance (∼100-fold photoswitchability of bioactivity, ∼1 μM *Z*-potency). However, north ring derivative **SBTub2M** (**15**) where a methyl group takes the space-filling position, had excellent *Z*-potency (*Z*-IC_{50} 35 nM) while also having excellent photoswitchability of bioactivity (ca. 200-fold; Figure 2a). This makes it the most potent and the most photoswitchable of the photoswitchable antimitotics known. **16** (methyl at the small polar position) and **14** and **18** (methyl projecting to inner face, clashes with protein) were predictably weaker than **SBTub2M** (though **16** still has submicromolar *Z* activity and ca. 100-fold switching), while **17** that projects the methyl to the outer face (toward the exit tunnel) was well tolerated (0.2 μM) and retained nearly 200-fold switching. It was pleasing that this SAR also followed the SAR known for **CA4**, as this supports that their target and binding site are conserved.

Our second priority was to develop soluble **SBTubs** for *in vivo* use in multiorgan animal models, which do not easily tolerate even low amounts of organic cosolvents, and which may require temperatures below those of typical 2D cell cultures (e.g., <30 °C for zebrafish). We aimed to formulate water-soluble **SBTub** prodrugs by phenol phosphorylation—an approach that has been successful for other colchicinoid inhibitors (including clinically advanced **CA4P**, **BNC105P**, etc).[37] We had initially produced **SBTub3P**, the phosphate prodrug of previous lead compound **SBTub3**, however, its aqueous solubility was only moderate (<2 mg/mL) potentially due to aggregate formation by π-stacking of the planar compound. We synthesized **SBTubA4P** hoping that the out-of-plane central methoxy group would reduce π-stacking, which combined with the hydrophilicity of the three extra methoxy groups would give better solubility, as we have seen in other contexts.[6,19] Indeed, **SBTA4P** dissolved to at least 10 mM in water at 25 °C, which was to prove important in later assays. Both prodrugs **SBTubA4P** and **SBTub3P** had similar cellular *Z*/*E* potencies as their drug forms.

In summary, we had developed **SBTubA4** and **SBTub2M** as mid-nanomolar antimitotics with 30−200-fold photoswitchability of bioactivity for cell culture studies (both cross-validated on A549 lung carcinoma cell line, Figure S5); and we had further developed **SBTubA4P** as a convenient fully water-soluble prodrug of **SBTubA4** for *in vivo* applications. These became the focus of our further biological evaluations.

2.2. SBTub Photoswitch Performance Studies. The photoresponses of most **SBTub**s (**1**−**5** and **9**−**20**) were similar to previously reported SBTs **SBTub2**/**3**,[18] with absorption maxima and absorption cut-offs being excellently balanced for both efficient $E \rightarrow Z$ photoswitching with the common 405 nm microscopy laser, and for full orthogonality to GFP imaging (ca. 488 nm). The separated $\pi \rightarrow \pi^*$ absorption maxima for *E*-(∼360 nm) and *Z*-isomers (∼330 nm) enable efficient directional $E \rightarrow Z$ photoisomerization at 360−420 nm reaching ca. 80% *Z* (Figure 2b), and extinction coefficients at 405 nm were up to twice those of similar azobenzenes, promising high-efficiency photoactivation on the confocal microscope. Importantly, *E*- and *Z*-SBT absorptions drop sharply toward zero above 410 nm (Figures 2c, S1, and S2) which is crucial for avoiding photoresponse to 488 nm GFP imaging under high-intensity focussed lasers, as well as with broader filtered excitation sources e.g., 490 ± 25 nm: since absorption "tails" extending far beyond band maxima can otherwise cause substantial photoswitching. (For example, 561 nm RFP imaging on the confocal microscope photoisomerizes azobenzene **PST-1** despite its extinction coefficients being less than 30 cm^{-1} M^{-1}.[24]) However, the **SBTubs**' cutoff suggested they would indeed be GFP-orthogonal, which was later confirmed and found to be crucial for *in vivo* use (see below).

In biological settings (>360 nm) and on the population level, these SBTs act similarly to photoactivation probes: (i) illuminations all give similar majority-*Z* equilibrium photostationary states (PSSs) in the photoresponsive spectral region (360 to ca. <440 nm), and (ii) they show no significant (<2%) $Z \rightarrow E$ thermal relaxation after hours in physiological buffers at pH ∼ 7 at 25 °C (Figures S3 and S4). However, they have all of the other practical advantages of photoswitches that are relevant to most research uses[38] (no toxic/phototoxic byproducts, fast illumination response, no nonoptical drug activation mechanisms, and stocks can be quantitatively relaxed to *E* by warming to 60 °C, which is advantageous for stock handling over sequential assays). Their photostability to continuous illumination at >380 nm was excellent. These features are shared with previously reported **SBTub2**/**3**.[18]

We used *ortho*-hydroxy **6** and *para*-amino **7** to test if strong electron donor groups that can tautomerize to freely rotatable

https://doi.org/10.1021/jacs.2c01020
J. Am. Chem. Soc. 2022, 144, 5614−5628

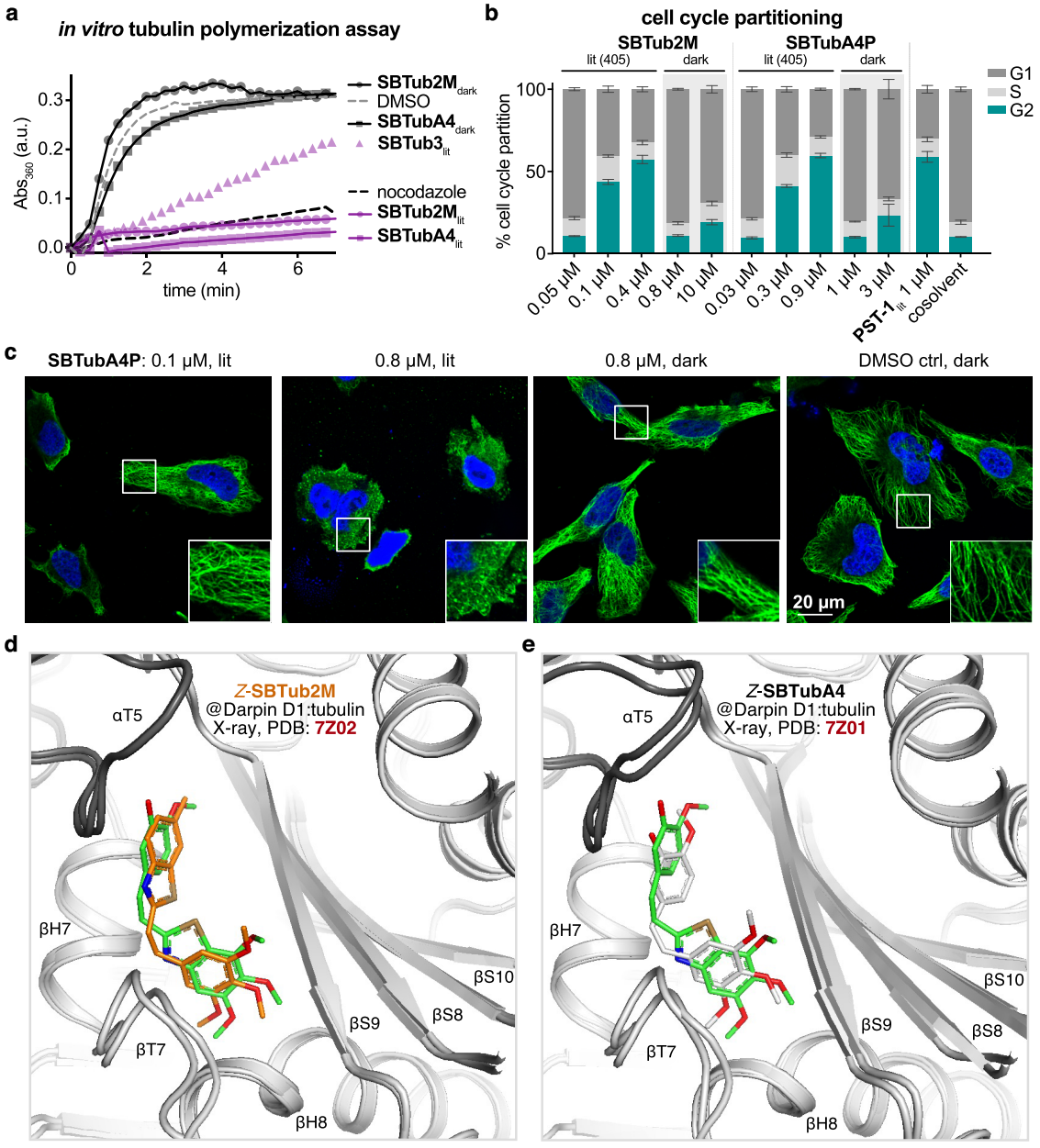

Figure 3. Tubulin-specific cellular mechanism. (a) **SBTubs** light-dependently inhibit tubulin polymerization (turbidimetric cell-free assay; absorbance mirrors the extent of polymerization; lit indicates majority-*Z*-**SBTub** (20 μM) preisomerized to PSS at 405 nm; nocodazole control at 10 μM). (b) Cell cycle analysis of Jurkat cells treated with **SBTub2M**/**SBTubA4P** matches photoswitchable reference **PST-1**: with significant G_2/M arrest under 405 nm pulsing (lit), but without cell cycle effects in the dark (matching cosolvent controls). (c) Immunofluorescence imaging of cells treated with **SBTubA4P** under pulsed 405 nm illuminations (lit, mostly-*Z*) and in the dark (all-*E*), compared to cosolvent control (HeLa cells, 20 h incubation; α-tubulin in green, DNA (stained with 4′,6-diamidino-2-phenylindole, DAPI) in blue). (d) Close-up views at the colchicine-binding site of X-ray co-crystal structures (PDB 7Z01, 7Z02) of *Z*-**SBTubA4** (green) and *E*-**SBTub2M** (orange) bound to the Darpin D1:tubulin complex (dark gray α-tubulin, light gray β-tubulin in cartoon representation; *Z*-**SBTubA4** and *Z*-**SBTub2M** in stick representation, oxygens red, nitrogen blue, and sulfur yellow). (e) Superimposition of tubulin:**CA4** (white carbons; PDB 5LYJ) and TD1:*Z*-**SBTubA4** (PDB 7Z01) shows that lead SBTubs share the same binding site as the parent natural product **CA4** (see also Figure S11).

quinoids (C−C single bond instead of C═C), can accelerate thermal $Z \rightarrow E$ relaxation to make better-reversible **SBTubs**; and if these would induce spectral red-shifting. However, in a cuvette, *Z*-**6**/**7** thermally relaxed only slowly (half-lives ≫ hours), and since *Z*-**7** gave similar cytotoxicity in the long-term cellular assay as its isostere **SBTub3**, we concluded that its cellular relaxation was not fast on a biological timescale either. The spectra of **7** were red-shifted by nearly 60 nm compared to typical SBTs putting the *E*-**7** absorption maximum exactly at the 405 nm laser line (Figure S1); however, as neither **6**/**7** brought relaxation rate benefits, we did not pursue them in this study.

Styrylthiazoles as in **8** have not yet been studied as scaffolds for photopharmaceuticals.[16] We were pleased that its isomers' spectra were only ca. 25 nm blue-shifted compared to the SBTs (giving less efficient isomerization at 405 nm), and all other properties, such as its completeness of $E \rightarrow Z$ photoswitching, were similar to the SBTs. We believe this opens up new possibilities for GFP-orthogonal, metabolically resistant photoswitches that are isosteric to azobenzenes, and so can replace

https://doi.org/10.1021/jacs.2c01020
J. Am. Chem. Soc. 2022, 144, 5614−5628

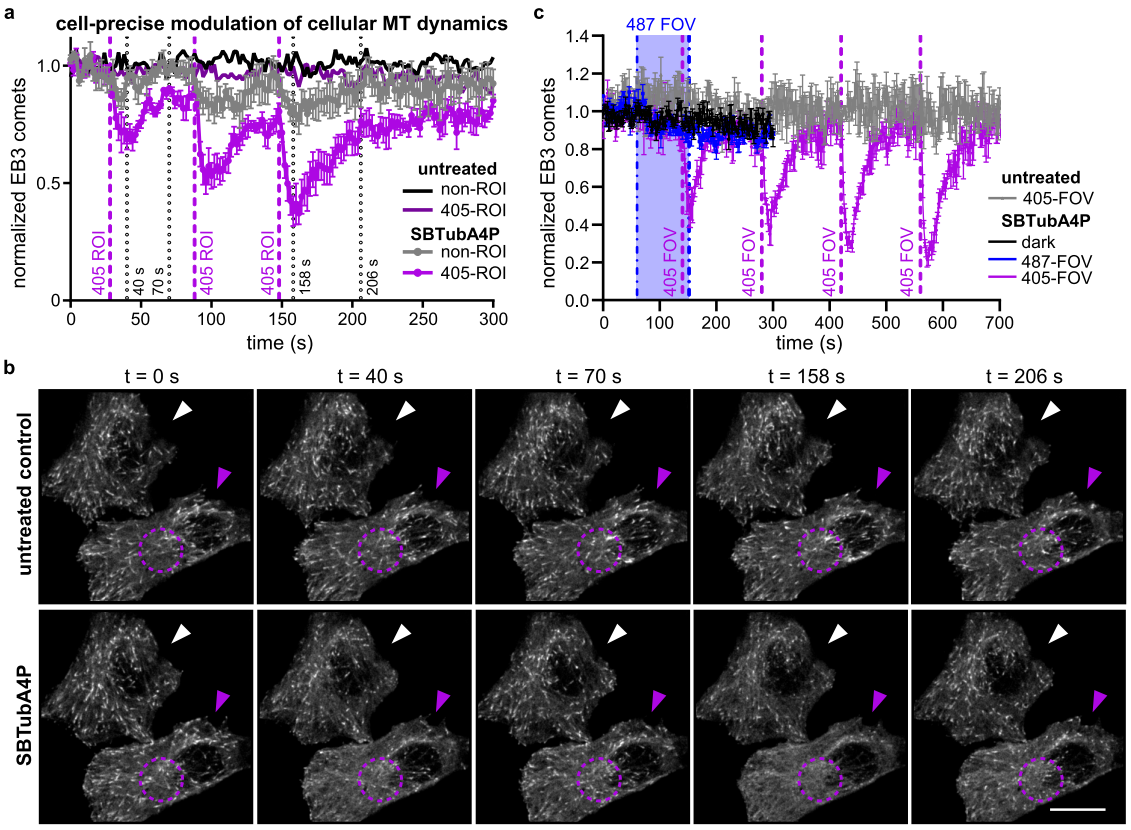

Figure 4. Spatiotemporal control over MT dynamics in 2D-cultured HeLa cells. (a, b) MT inhibition in **SBTubA4P**-treated cells is initiated only upon 405 nm illumination pulses and only in ROI-targeted cells (data related to Movie S1; live-cell EB3-tdTomato comets quantify polymerizing MTs). (a) Comet count statistics are similar to cosolvent-only baseline in both ROI-pulsed-cosolvent and non-ROI-**SBTubA4P** conditions; ROI-**SBTubA4P** statistics show inhibition spikes. (b) Stills from Movie S1 at the times indicated in (a), initially during the untreated timecourse, then during the **SBTubA4P**-treated timecourse on the same cells. Purple arrowhead indicates the ROI cell; purple dotted circle indicates where the 405 nm ROI is applied at times 26, 88, and 148 s; and white arrowhead indicates the non-ROI cell quantified as the internal control (scale bar 15 μm). (c) EB3 comet counts of cells imaged at 561 nm only (dark, gray), with 47 frames at 487 nm applied to full field of view during the time span indicated with dashed lines ("487", cyan) and **SBTubA4P** (6 μM), or with single-frame 405 nm pulses, **SBTubA4P** (0.6 μM), applied to full field of view at times indicated with dashed lines ("405", violet) (n = 3 cells). Temporally precise onset and full-field diffusional reversibility are shown (data related to Movies S2 and S3). [(a, c) Mean ± standard error of the mean (SEM) EB3 comet counts as normalized to the means of the first five time points; 405 nm ROIs applied at indicated times; for further details, see the Supporting Information].

them for applications where these biologically advantageous properties are required.

For all further details, including full discussion of photoswitch performance of **6**/**7** and of *E*-**SBTub** toxicity, see the Supporting Information including Figures S1−S5.

2.3. SBTubs Isomer-Dependently Target Tubulin in Cells. To test their cellular mechanism of bioactivity, we first examined the **SBTubs**' isomer-dependent inhibition of polymerization of purified tubulin protein in a cell-free assay. Both leads **SBTubA4** and **SBTub2M** were noninhibiting in the all-*E* dark state, allowing tubulin to polymerize as in the cosolvent control (Figure 3a). However, in the majority-*Z* illuminated state, they were potent inhibitors that suppressed polymerization entirely to baseline readout levels, comparable to the archetypical colchicinoid nocodazole. Matching the antiproliferation assays, they were significantly stronger inhibitors than first-generation **SBTub3** (Figure 3a).

If microtubule inhibition is also the main cellular mechanism of action of *Z*-**SBTubs**, we would expect *Z*-**SBTub**-treated cells to show G_2/M-phase cell cycle arrest due to mitotic checkpoint failure.[15] We therefore used flow cytometry-based analysis to quantify cell cycle repartition. *E*-**SBTubs** caused either no change or small changes compared to controls, whereas G_2/M arrest was strongly induced by *in situ* lit (mostly-*Z*) **SBTubA4P** and **SBTub2M** (Figures 3b and S6).

As G_2/M-phase arrest is necessary but insufficient to conclude on cellular tubulin inhibition being their major mechanism of action, we next performed confocal microscopy imaging of the MT network architecture in immunofluorescently stained cells, to directly observe tubulin-inhibiting effects. *In situ* illuminated **SBTubA4P** caused microtubules to curve and MT architecture to break down,[39] but *E*-**SBTubs** caused no disorganization at corresponding concentrations in the dark, matching cosolvent controls (Figure 3c). This matches the assumption that their photoswitchable cytotoxicity arises from their *Z*-isomers potently inhibiting MT dynamics and stability in cells. While microscopy is a qualitative method that can misrepresent population-level statistics, the quantitative cell cycle data from flow cytometry (10^4 cells per datapoint) as well as the qualitative match to previous **SBTub** work[18] give confidence to this result.

Finally, to check our design that *Z*-SBTubs act as colchicinoids, we crystallized the *Z*-**SBTubA4** and *Z*-**SBTub2M**:tubulin DARPin D1 (TD1) complexes. X-ray diffraction studies showed that both *Z*-**SBTubA4** and *Z*-**SBTub2M** indeed directly bind tubulin at the colchicine site very similarly to **CA4**, even with the same orientation of its

https://doi.org/10.1021/jacs.2c01020
J. Am. Chem. Soc. 2022, 144, 5614−5628

substituents (Figures 3d,e and S11; data deposited as PDB 7Z01 and 7Z02). This explains why the **SBTub** SAR determined in this study (Table 1) mirrors that known for **CA4**. It also highlights the plasticity of the binding site, which accepts such differently sized inhibitors.

Taken together, these cell-free and cellular assays support that the **SBTubs** act as light-dependent tubulin inhibitors in cells, with their *Z*-isomers binding potently at the colchicine-binding site and their *E*-isomers having no effects at the corresponding concentrations.

2.4. SBTub Photocontrol Enables Cell-Precise, Temporally Reversible MT Inhibition in 2D Cell Culture. Aiming later to apply **SBTubs** to photocontrol MT dynamics in complex models and *in vivo*, we now switched to using the fully water-soluble prodrug **SBTubA4P**. This is an important step: (i) it avoids cosolvents that can be problematic for *in vivo* toxicity and (ii) it prevents hydrophobic adsorption onto the matrix materials (PDMS, collagen, agarose) that are used in 2D structured surfaces, 3D cell culture/organoid models, and for embedding motile animals during long-term imaging. Avoiding adsorption is important in our experience, as hydrophobic compounds can exhibit irreproducible apparent potencies or effects in these settings, which is timewise- and ethically prohibitive for resource-intensive low-throughput animal studies.

Before performing animal work, we probed the spatiotemporal resolution that **SBTubs** could achieve for *in situ*photoswitching-based control over MT dynamics, in 2D cell culture. Using spinning disk confocal live-cell microscopy, we imaged **SBTubA4P**-treated cells transfected with a fluorescently labeled fusion of the MT end binding protein EB3, to directly monitor MT polymerization dynamics during photoswitching.[18] This is possible since EB3 labels the GTP-cap of MTs, so EB3-tdTomato acts as a fluorescent marker revealing the tips of polymerizing MT plus ends in cells as hundreds of dynamic "comets" that cascade through the cell at significant velocities (tdTomato excitation at 561 nm).[40] Our protocol for cell-precise photoswitching of MT dynamics, with internal controls for compound application and for photobleaching, was as follows. We imaged transfected cells before **SBTubA4P** application to establish untreated MT dynamics baselines, simultaneously controlling for effects of 405 nm laser pulses on single selected cells [targeted by region of interest (ROI) illumination]; then, we added *E*-**SBTubA4P** to these same cells and continued imaging the whole field of view while applying targeted pulses of the 405 nm laser to a single ROI-selected cell.

SBTubA4P enabled repeatable cycles of temporally reversible, photoswitching-induced inhibition of MT dynamics in live cells, with single-cell spatial targeting precision and second-scale onset time precision (Figure 4a,b and Movie S1). In **SBTubA4P**-treated ROI cells, within seconds upon each single-frame 405 nm pulse, polymerizing MT tips stop moving and disappear, then more slowly reappear and resume movement (best seen in Movie S1). Statistics collected over multiple independent experiments showed these inhibition spikes are highly reproducible; recovery toward uninhibited baseline has a half-life of ca. 25 s, which we attribute to the diffusion of *Z*-**SBTub** out of the ROI cell (Figure 4b). There were minor effects on MT dynamics in treated non-ROI neighbor cells compared to pre-treatment controls, and the 405 nm pulsing protocol alone did not cause any readout changes (Figure 4a).

We also modified this protocol to apply single-frame 405 nm pulses to the whole field of view instead (Figure 4c and Movie S2). As expected, this confirmed the temporal precision of onset and the temporal reversibility of the spiking seen with the single-cell-resolved studies; though the video data are easier to interpret as they are even more visually impressive (Movie S2). Finally, we performed full-field-of-view imaging while applying a train of 47 frames of 487 nm pulses, to test whether **SBTubA4P** can be used orthogonally to GFP imaging wavelengths. Indeed, even at this high concentration (6 μM, 40× $[I]_{WC}$), there was no induction of MT inhibition, so we concluded that **SBTubA4P** is indeed GFP-orthogonal, matching our design (Movie S3 and Figure 4c).

2.5. From Cell Culture to MT Photocontrol in 3D Models, Tissue Explants, and Animals. By now we had optimized the potency of metabolically stable, GFP-orthogonal photoswitchable **SBTub2M** and fully water-soluble analogue prodrug **SBTubA4P**, clarified the **SBTubs**' tubulin-specific cellular mechanism of action, and shown high-spatiotemporal-resolution photocontrol of MT dynamics in 2D cell culture. We were now primed to tackle the central photopharmacology research challenge, which has so far frustrated essentially all prior approaches: *in vivo* translation using systemic administration but local photocontrol, that clearly and usefully retains a defined cellular mechanism of action. We set out to test if **SBTubs**' performance features would allow this operation across a range of complex models from 3D culture, to 3D tissue explant, to two *in vivo* animal models: with spatiotemporally localized illuminations photocontrolling the full sequence of their bioactivity (from suppressing MT polymerization to altering/depolymerizing MT network structures and to reducing/stopping microtubule-dependent downstream processes), where appropriate with second-level resolution, but all with cellular precision.

2.6. SBTub Photocontrol in 3D Organoids Enables Spatially Targeted Blockade of Migration and Mitosis in the Long Term. We first tested **SBTubA4P** in 3D human mammary gland organoids grown from isolated patient tissue embedded in collagen gels. These resemble miniaturized and simplified organs with realistic micro-anatomy, and feature collective motility/invasion behavior directing cells to migrate and proliferate to form ordered, branched structures.[41,42] Controlling organoid morphology is a sought-after goal, which has been mostly interpreted as requiring spatiotemporal control of gene expression, for which optogenetic approaches have been suggested.[43] Yet, the spatiotemporally localized application of photochemical compounds offers an alternative, in which the possibility of instantaneous cellular response to stimulus is highly attractive for temporally precise control. Based on the good performance of **SBTubA4P** in 2D cell culture, we assessed whether **SBTubA4P** can be controlled similarly precisely in a 3D organoid model, aiming to manipulate organoid development by locally interfering with the invasion of individual branches during the elongation phase.[42]

Though the actin cytoskeleton is the major driver of cell migration, MTs are integral to directional migration and leading-edge stabilization[24,44,45] (as well as to proliferation): so we expected the single-cell motility as well as cell division rates could be locally affected. Therefore, we wished to test if repeated localized photoactivations of **SBTubA4P** (every 7 min) could be used over long timescales (>24 h) to inhibit outgrowth of light-targeted organoid branches, while leaving other branches of the same organoids to develop: so shaping and modulating cell

https://doi.org/10.1021/jacs.2c01020
J. Am. Chem. Soc. 2022, 144, 5614−5628

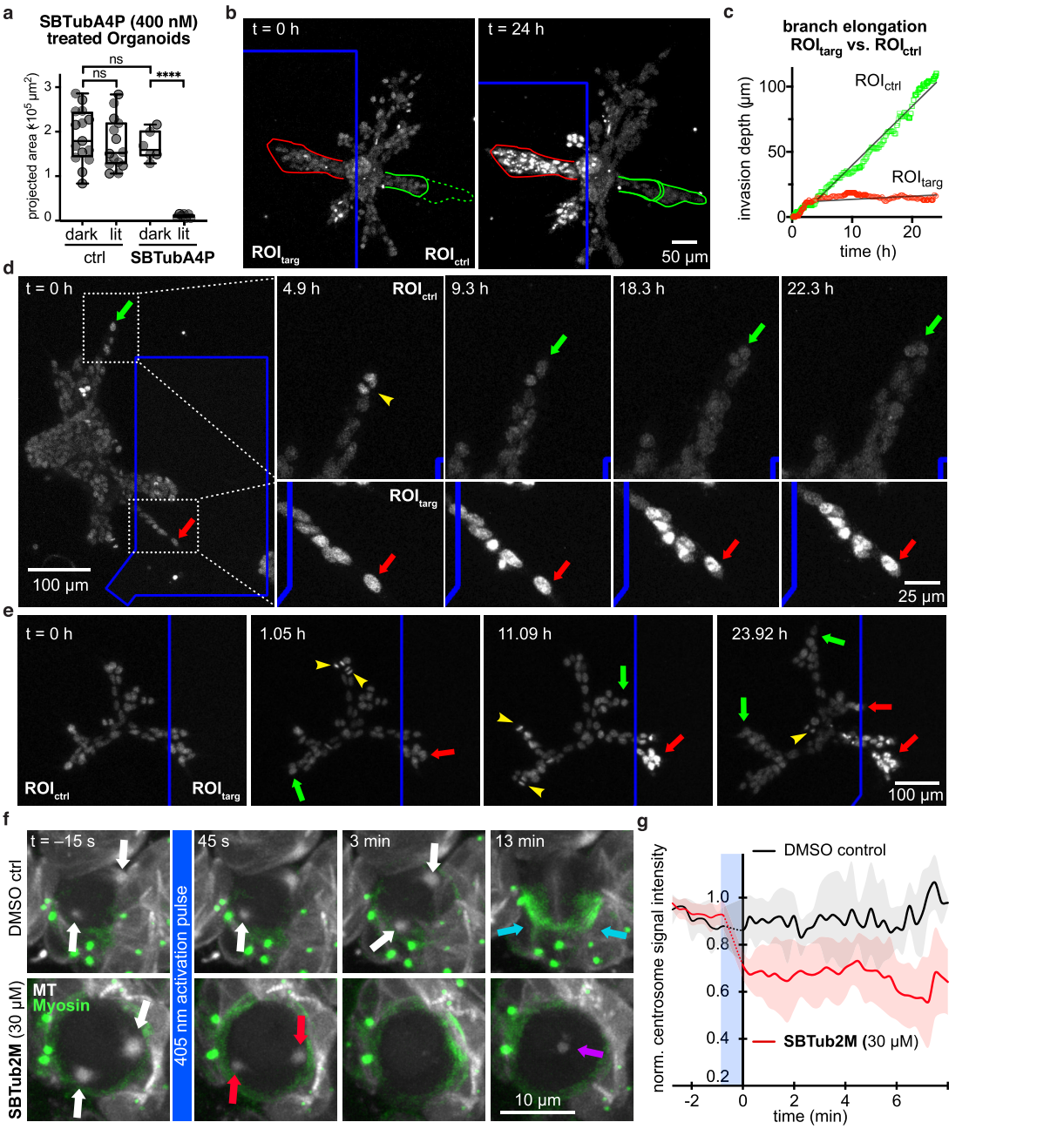

Figure 5. Spatiotemporal control over MT architecture, migration, and mitosis in 3D culture and tissue explant. (a) 3D human mammary gland organoids embedded in collagen gels only have inhibited branch outgrowth when treated with both **SBTubA4P** and UV pulses. (b) Local applications of UV light to ROI_{targ} regions of **SBTubA4P**-treated organoids (blue box, one ca. 450 ms pulse per 7 min per z-stack) stops branch proliferation and outgrowth (red outline), while branches in untargeted ROI_{ctrl} regions develop dramatically (start: solid green line, final: dotted green line) (related to Movie S4). (c) Radial progress of branch tip fronts (directed and collective behavior) in ROI_{targ} and ROI_{ctrl} regions. (d) Still image timecourse, zoomed on a branch tip in the ROI_{ctrl} (blue box) region, showing cell proliferation (yellow arrowhead) and matrix invasion (one representative of the migrating cells is tracked over time with green arrows), while branch tip of ROI_{targ} region has static non-proliferating cells and even slight branch retraction (red arrows) (data related to Movie S5). (e) Branch progression and proliferation are unimpeded and continuous in ROI_{ctrl} regions, while ROI_{targ} regions are static, and branches growing into the ROI_{targ} stop their growth (color code as in (e), data related to Movie S6). [(a–e) Cell location in organoids tracked with nuclear stain SiR-DNA imaged at 647 nm]. (f) Whole-field-of-view 405 nm photoactivation of **SBTub2M**-treated intact 3D brain explants of larval *Drosophila melanogaster* (bottom row) causes neuroblast centrosomes (red arrows) to rapidly shrink in size and signal intensity (45 s and 3 min) and prevents the cell from progressing through division (13 min). Some MT signal accumulates at mid-cell at later time points (purple arrow) (data related to Movie S8). In DMSO-only controls (top row), centrosome integrity (white arrows, 45 s and 3 min) and progression through the cell cycle (13 min) are unaffected, indicated by myosin accumulation at the cleavage furrow (cyan arrows) (data related to Movie S9). [MTs in white (Jupiter::mCherry imaged at 561 nm), myosin in green (Squash::GFP imaged at 488 nm)]. (g) Relative mCherry fluorescence intensity of centrosomal ROIs in **SBTub2M**-treated prophase neuroblasts (red) after activation at 405 nm drops notably during the approximately 45 s activation period (blue box) compared to the DMSO control prophase neuroblasts (black). Signal intensities are shown as the proportion of the per-cell maximum preactivation signal intensity (shading indicates ±1 standard deviation, 1–2 centrosomes quantified from a total of five neuroblasts from three different animals). For details, see the Supporting Information.

https://doi.org/10.1021/jacs.2c01020
J. Am. Chem. Soc. 2022, 144, 5614–5628

migration and invasion with spatiotemporal control. This aim brings conceptual challenges for photopharmaceuticals: since all cells are exposed to the same drug concentration, and over long timescales the cumulative impacts of scattered photoactivation light, of the diffused isomerized compound, and of imaging light itself, may build a spatially nonspecific background pattern of bioactivity. Organoid morphology does not tolerate >0.1% organic cosolvent either, making full solubility important.

We first determined a suitable working concentration for **SBTubA4P** without spatially resolved activation, by monitoring organoid areas for morphological disruption under lit/dark conditions (Figure S7a). We determined an $[I]_{WC}$ of 200 nM for preventing organoid growth over 24 h with UV-lit **SBTubA4P**, whereas organoids treated at 400 nM but kept in the dark grew healthily with no antiproliferative/branch-retracting effects (Figures 5a and S7a,b).

Then, we applied localized UV ROI illuminations to selected organoid branches (ROI_{targ}) every 7 min, comparing to non-UV-illuminated internal control branches (ROI_{ctrl}). This allowed us to noninvasively block cell migration/invasion and proliferation with striking spatial resolution and long-term persistence. With **SBTubA4P**, the development of ROI_{targ} branches was totally blocked over >1 day (Figure 5b−d, Movies S4 and S5), while no-compound controls showed no photoinhibition of branch development (Movie S7 and Figure S7c). Control branches displayed high motility and matrix invasion (green outline, Figure 5b) and their cells freely proliferated (yellow arrowhead, Figure 5d), resulting in considerable branch development. The out-directed motion of the collective branch fronts was continuous in ROI_{ctrl} regions (ca. 4.5 μm/h) but was almost completely stopped in ROI_{targ} (ca. 0.2 μm/h; Figure 5c). Overall development of branches, only entering ROI_{ctrl} areas, was however clearly visible without any statistical analysis (Figure 5e and Movie S6). Thus, **SBTubA4P** can be used in 3D matrix cell culture settings to noninvasively control cell motility, invasion, and proliferation, allowing photopatterning of branch growth and organoid development down to the spatial scale of individual cells.

2.7. SBTub Photocontrol in Intact 3D Tissue Explants Allows Temporally Precise MT Depolymerization and Mitotic Control in the Short Term. We next tested **SBTub** performance and tubulin-specific mechanism of action when directed against the more complex 3D environment of live intact brain lobes of early third instar larval *D. melanogaster* (fruit fly). Larvae are too motile for long-term imaging and the larval cuticle is largely impermeable, so neurodevelopment studies explant the whole brain. As the explant tolerates cosolvent, we took the opportunity to use **SBTub2M** in these assays to test the broader applicability of the **SBTub** design. Both the whole-organ and explant aspects bring significant challenges. (1) Compounds must permeate through two glia cell layers to reach mitotically active neural stem cells (neuroblasts). This forces the use of high bath concentrations and potent compounds: however, since surface and surrounding cells are exposed to far higher concentrations than central cells, only potent compounds with extremely high photoswitchability of bioactivity ("FDR"; discussed in ref 19) can be used: otherwise, outer cells die, and morphology and physiology are lost. Indeed, we could use high concentrations of high-FDR **SBTub2M** (30 μM) in brain explants without noticeable toxicity. (2) Using multiple fluorescent protein labels for multiplexed imaging is a typical requirement to achieve useful readouts in biology, but can block chemical photoswitch applications. The most common long-wavelength fluorescent proteins for animal work are excited at 561 nm, which forces the use of GFP (488 nm) or YFP (514 nm) fusions as the next-longest-wavelength markers. For example, to image both MTs and cellular structural elements, we used animals expressing the microtubule-binding protein mCherry::jupiter,[46,47] and cortical structure marker sqh::GFP (spaghetti squash, the regulatory light chain of the non-muscle type 2 myosin, fused to eGFP[48]). With hemithioindigo or azobenzene reagents, such two-channel FP imaging would isomerize the photoswitch throughout the sample due to photoresponse at ≤530 nm (Figure 2b), so destroying spatiotemporal specificity in the study zone. In contrast, the nonresponse of the GFP-orthogonal SBT to 488 nm imaging avoids any photoisomerization during typical two-channel FP imaging, allowing precise temporal control of activation in our experiments.

We transferred freshly dissected brain explants into 30 μM **SBTub2M** and started imaging after 30 min loading (Figure S8). We imaged in both mCherry (ex 561 nm) "red channel" and GFP (ex 488 nm) "green channel" for 15 min to establish baseline, then photoactivated **SBTub2M** throughout the imaging stack volume with 405 nm. Photoactivated **SBTub2M** depolymerized centrosome microtubules within 60 s (Figure 5f, Movies S8, and S9, MTs shown in white). To control for target specificity, we also used mCherry::tubulin[49] for imaging MTs, and observed similar behavior (Movies S10 and S11). As microtubules are rapidly nucleated in prophase centrosomes, we quantified the loss of centrosomal fluorescence signal after activation as a highly conservative estimate of centrosome MT depolymerization. We saw dramatic, temporally resolved signal reduction at the approx. 45 s activation period, while **SBTub** controls were unaffected (Figure 5g). We used the second FP channel to image Sqh::GFP, a marker of the cell actomyosin cortex, which plays a key role in neuroblast asymmetric division.[50,51] Normally dividing neuroblasts accumulate Sqh::GFP at the cell cleavage furrow during anaphase. Neuroblasts in which **SBTub2M** was photoactivated retain uniform cortical myosin, indicating mitotic arrest in the absence of mitotic spindles[50] (cyan arrows, Figure 5f).

Previous short-term results imaging EBs at low **SBTub** concentrations in 2D cell culture had illustrated only its capacity to spatiotemporally block MT polymerization (Figure 4). Now, these useful results in the intact brain underlined that **SBTub2M** maintains its *Z*-isomer-specific, MT-depolymerizing mechanism of action in live tissue explant, casting **SBTubs** as flexible and powerful tools for cytoskeleton photomanipulation in complex 3D settings.

2.8. SBTub Photocontrol in Live Animals Enables Targeted Blockade of Embryonic Development. Encouraged by performance in 3D models, we evaluated using **SBTubs** for *in vivo* photocontrol in intact animals. First, we studied the effects of *in situ* photoactivations of **SBTubA4P** on the development of *Xenopus tropicalis* clawed frog embryos. During the initial 48 h of development, embryos normally transition over many division cycles from cell spheres through the blastula stage through to multi-organ tadpoles (Figure S9a). Initially, we tested the effects of **SBTubA4P** in the earliest stages of development, just after embryonic divisions had started, by treating 2-cell stage embryos with *E*-**SBTubA4P** (1 h loading, then medium exchange and optional *in situ* embryo-localized 410 nm photoactivation pulse during washout; note that this transient exposure to the **SBTub** parallels what could be expected for e.g., systemic i.v. administration in mammalian

https://doi.org/10.1021/jacs.2c01020
J. Am. Chem. Soc. 2022, 144, 5614−5628

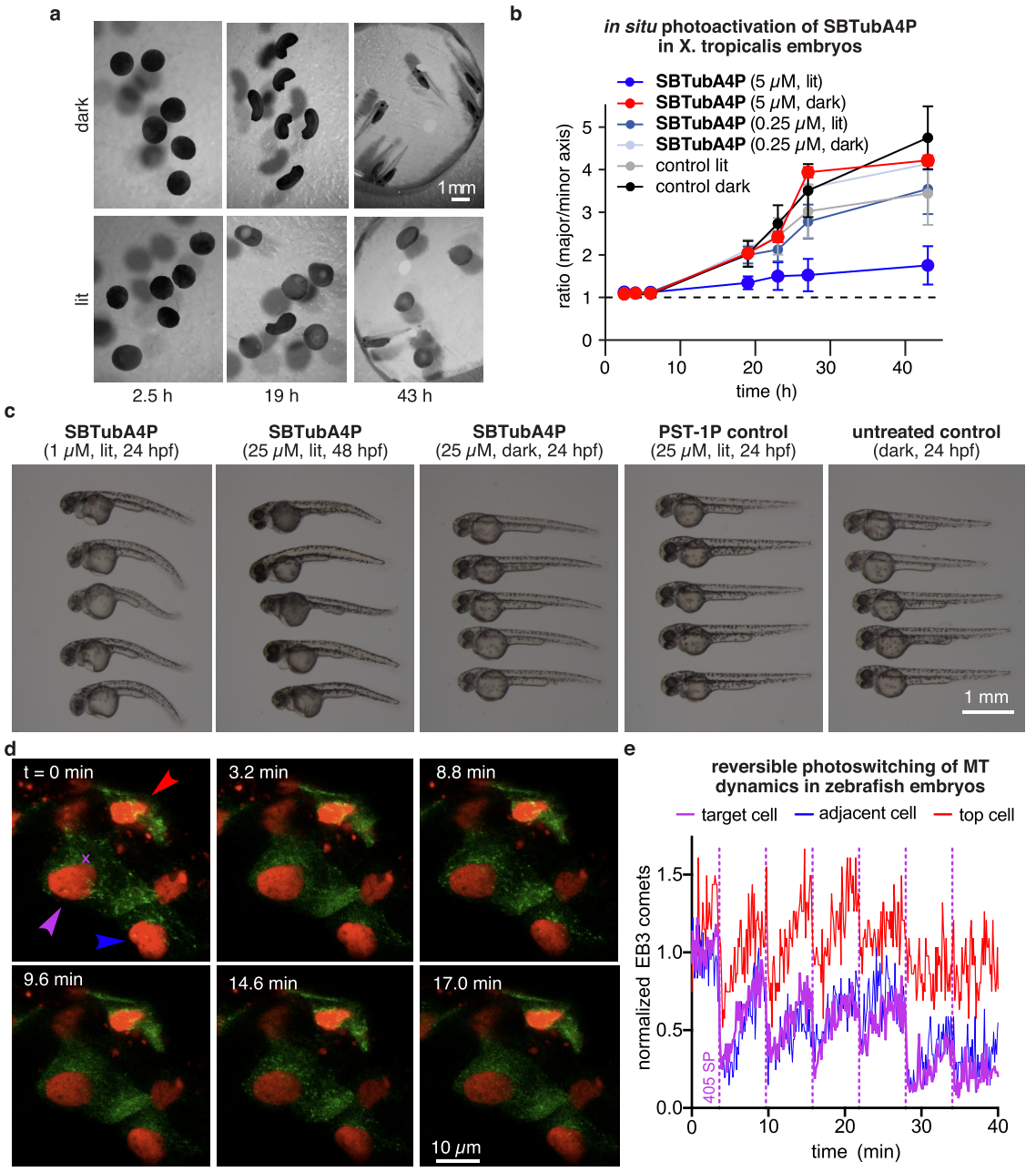

Figure 6. Photoinhibition of *X. tropicalis* development, and *in vivo* photocontrol of MT dynamics in *Danio rerio*. (a, b) *Xenopus* embryos incubated with compounds for 1 h at the two-cell stage, before medium exchange optionally with 410 nm photoactivation. Embryos show irreversible development inhibition by *in situ* formed *Z*-**SBTubA4** in lit conditions but had no effects in the dark or with a low concentration of **SBTubA4P** [(a) **SBTubA4P** at 5 μM; (b) development quantified by the ratio of major to minor embryo axis lengths, six embryos per condition, mean ± SEM]. (c) Development of *D. rerio* treated at the indicated stages for 24 h with **SBTubA4P** or control compounds under dark or pulsed lit (1 s/5 min) conditions. **SBTubA4P** (1 or 25 μM) causes morphological abnormalities only in the lit state, showing that it remains effective *in vivo*. (d, e) Reversible modulation of MT dynamics in 48 hpf zebrafish embryo (25 μM). (EB3-GFP in green, histone H2B in red). (data related to Movies S12−S16; see the Supporting Information).

models—further discussion in the Supporting Information). Embryos only failed to develop morphologically over the subsequent 2 days if they had received the 410 nm photoactivation; embryos without photoactivation developed normally (Figure 6a,b). We also tested interfering with development at the later blastula stage (>64 cells) by a similar protocol. While subsequent morphological development was normal under lit and dark conditions (Figure S9b,c), sensorimotor responses to mechanical stimulation[52] were suppressed by lit **SBTubA4P** only (Figure S9e and Movie S12). Interestingly, the tubulin-inhibiting azobenzene photoswitch **PST-1P** (Figure S9d) light-independently suppresses sensorimotor responses. We believe the SBT's success may reflect its greater metabolic robustness (see the Supporting Information); and at any rate, it indicated that **SBTubs** are suitable for *in vivo* use.

2.9. SBTub Photocontrol in Live Animals Enables Cell-Precise Temporally Reversible Inhibition of MT Dynamics. Finally, we switched to highly spatiotemporally resolved *in vivo* MT-imaging studies that would test **SBTubA4P**'s mechanism of action and applicability in the zebrafish *D. rerio*, when systemically applied and maintained in the bath medium.

https://doi.org/10.1021/jacs.2c01020
J. Am. Chem. Soc. 2022, 144, 5614−5628

We first determined useful working concentrations in zebrafish, incubating 24 and 48 hpf (hours post fertilization) embryos in **SBTubA4P** under lit and dark conditions for 24 h. While zebrafish morphology remained unaltered in all dark **SBTub** treatments, 24 hpf embryos treated with lit **SBTub** showed major morphological changes even down to 1 μM, whereas more developed 48 hpf embryos showed similar morphological changes only at higher **SBTubA4P** concentrations e.g., 25 μM (Figures 6c and S10). Again, we compared these effects to those of azobenzene reagent **PST-1P**, now observing a dramatic difference: even 25 μM lit **PST-1P** did not interfere with development at either the 24 hpf or 48 hpf stage (Figures 6c and S10). This argues still more conclusively than Figure 6b, that the SBTub scaffold is uniquely suitable for light-controlled biological effects, compared to the previously known azobenzene scaffold. Finally, we checked the lower-potency soluble prodrug **SBTub3P** in the same assay; matching expectations, it caused only weak changes at 24 hpf and no visible changes at 48 hpf (Figure S10), showing the necessity of the potency optimizations we performed in this study.

Aiming to test the MT-modulating effects of **SBTubs** in a challenging live animal system, we therefore decided to proceed with 48 hpf zebrafish embryos, and an **SBTubA4P** working concentration of 25 μM. We took 48 hpf embryos coexpressing EB3-GFP and histone H2B-mRFP as a nuclear marker,[53,54] loaded them with 25 μM *E*-**SBTubA4P** for 4 h, then washed and embedded them in agarose. Imaging at 488 nm caused no suppression of EB3 comets, confirming **SBTubA4P**'s GFP orthogonality *in vivo*. However, photoactivation with the 405 nm laser at a single point caused EB3 comets to vanish rapidly in cells around the targeted region, recovering over ca. 10 min. Cells further from the targeted region were predictably less inhibited than those with direct contact to the photoactivation region. The photoactivation-recovery cycle could be repeated multiple times during imaging (Figure 6d,e and Movies S13–S16). Not only microtubule polymerization dynamics but also mitotic progression, could be stopped by spatiotemporally localized **SBTubA4P** photoactivation *in vivo* (Movie S16). These experiments confirm that the SBT scaffold, in general, is viable for light-triggered *in vivo* studies, and that **SBTubA4P** when applied *in vivo* retains its mechanism of action as a potent, light-dependent MT inhibitor with excellent spatial specificity and satisfying temporal reversibility.

3. CONCLUSIONS

Noninvasive optical tools to modulate microtubule dynamics, structure, and function with high precision offer unique potential in the many fields of biology impacted by the spatiotemporally resolved processes that MTs support, such as cargo transport, cell motility, cell division, development, and neuroscience. Photopharmaceutical chemical reagents are conceptually elegant optical tools in that they can be rapidly transitioned across models and settings and that they can be rationally designed for photoresponse patterns that interfere minimally with imaging while maximizing optical response to a chosen photoactivation wavelength. Locally applied photopharmaceuticals, particularly intraocularly applied reagents for action potential control in the retina, have made great progress in adult mammalian disease models.[55,56] However, reaching general uses of photopharmacology involving precise targeting of drug activity *in vivo* by localized *in situ* photoactivations following systemic administration remains an unsolved challenge for photopharmaceuticals with cytosolic target proteins. This would require combining high photoswitchability of bioactivity, high potency, metabolic robustness, aqueous solubility, and imaging orthogonality. Indeed, very few systemic *in vivo* applications of photopharmaceuticals have been made, and to date, no *in vivo* studies have combined testing a defined mechanism of drug action, with exploring the potential for cell-scale spatially resolved targeting following systemic administration.[57−59] Thus, the ability of photopharmacology to contribute useful systemically applicable reagents for organism studies has remained unclear.

In this work, we develop highly light-specific tubulin polymerization inhibitors with unprecedented applicability from 2D cell culture, through 3D culture and whole-organ explant, to systemic *in vivo* administration with local photoactivation. Realizing that the metabolic robustness and imaging orthogonality of a photopharmaceutical largely depend on its photoswitch scaffold, we consciously selected the recently developed SBT photoswitch and screened a SAR panel of 20 **SBTubs**. We optimized the potency and photoswitchability of bioactivity in lead **SBTub2M**, and we solubilized another lead to create **SBTubA4P**, which does not require organic cosolvents. **SBTubs** are efficiently photoactivated with the common 405 nm laser, but their sharp absorption cutoff leaves GFP, YFP, and RFP channels free for multiplexed imaging of fusion protein markers without risking compound photoactivation. This is a highly desirable feature for areas of research where photopharmacology's optical precision can best contribute unique solutions on the cellular spatial scale (although this practical use logic does run counter to the goal of "photoswitch red-shifting" that is often cited in chemical design). We cross-validated the **SBTubs**' molecular mechanism of action in cell-free, cellular, and *in vivo* settings. **SBTubs** light-dependently interfere with mitosis in cell culture, and *in vivo* they depolymerize mitotic spindles, ultimately blocking development. They can be optically patterned to control motility and branch development in 3D organoid cultures, and their photocontrol allows rapid response, cell-specific inhibition of microtubule dynamics in cell culture and *in vivo*.

These consistent results across a range of models at different scales of time, length, and biological complexity recommend the **SBTubs** as excellent and unique general-purpose tools for optically manipulating microtubule dynamics, microtubule structure, and microtubule-dependent processes with high spatiotemporal precision.

The proof-of-concept biological performance of the **SBTubs** has been very satisfying. We believe that the most valuable improvement to this system will now be to extend the temporal reversibility of inhibition (seen in 2D cell culture by diffusion to the medium with ca. 20 s half-time, Figure 4) to whole-organ/whole-animal settings. In these settings, diffusion is slower to achieve reversibility (ca. 10 min), so we seek techniques for *in situ* bidirectional isomerization of **SBTubs** in our ongoing research. We believe that bidirectional photoswitching may be difficult within the biologically compatible wavelength range.[16] However, accelerating thermal relaxation to the minute scale, which is probably the most appropriate scale for 3D/*in vivo* applications of interest, may be feasible, and efforts are underway.

In conclusion, the **SBTubs** are excellent photoswitchable microtubule-depolymerizing reagents for use in cell culture, 3D culture, small explant, and early-stage animals. Their potency, flexibility, and ease of use recommend them for high-spatiotemporal-precision research across cytoskeleton biology;

https://doi.org/10.1021/jacs.2c01020
J. Am. Chem. Soc. 2022, 144, 5614−5628

particularly, we feel, for cell-specific applications to motility and development, but they will also be of great interest in cargo transport, biophysics, cell polarity, neurodegeneration, and cell division. Finally, we expect that by supporting conceptual innovations in photoswitch scaffold chemistry and rational photopharmaceutical design, and particularly by starting to unlock the applications promise of photopharmacology for globally administered, locally targeted *in vivo* use, this **SBTub** research represents a promising advance for high-performance photopharmacology against other protein targets in general, beyond their immediate impact on microtubule biology.

■ ASSOCIATED CONTENT

Supporting Information

The Supporting Information is available free of charge at https://pubs.acs.org/doi/10.1021/jacs.2c01020.

Temporally precise and cell-precise inhibitions of cellular MT polymerization dynamics by photoactivations of *E*-**SBTubA4P** at 405 nm (Movie S1) (MP4)

Temporally precise full-field-of-view inhibitions of cellular MT polymerization dynamics by photoactivations of *E*-**SBTubA4P** at 405 nm (Movie S2) (MP4)

No inhibition of cellular MT polymerization dynamics by illumination of *E*-**SBTubA4P** at 487 nm (Movie S3) (MP4)

SBTubA4P blocks branch development in primary human mammary gland organoids, light-dependently and with spatiotemporal precision (Movies S4−S6) (MP4, MP4, MP4)

No-compound control shows no photoinhibition of organoid branch development in both ROI_{targ} and ROI_{ctrl} (Movie S7) (MP4)

Temporally precise depolymerization of the mitotic spindle in a prophase Drosophila neuroblast by photoactivation of *E*-**SBTub2M** (30 μM) at 405 nm (Movie S8) (MP4)

DMSO-only control to Movie S8 shows prophase Drosophila neuroblast undergoing normal mitosis after 405 nm illumination (Movie S9) (MP4)

Temporally precise depolymerization of the mitotic spindle in a prophase Drosophila neuroblast by photoactivation of *E*-**SBTub2M** (30 μM) at 405 nm (Movie S10) (MP4)

DMSO-only control to Movie S10 shows prophase Drosophila neuroblast undergoing normal mitosis after 405 nm illumination (Movie S11) (MP4)

Reaction of hatchling frog *X. tropicalis* embryos to mechanical stimulus depends on the temporally precise application of *Z*-**SBTubA4** during prior development (Movie S12) (MP4)

Photoactivation of **SBTubA4P** (25 μM) in a live zebrafish embryo shows temporally reversible inhibitions of EB3 dynamics over several cycles (Movies S13 and S14) (MP4, MP4)

Inhibition of MT polymerization dynamics in zebrafish embryo when **SBTubA4P** (25 μM) is photoactivated (Movie S15) (MP4)

Photoactivation of **SBTubA4P** (25 μM) stops both EB3 dynamics and cell division in the developing zebrafish embryo (Movie S16) (MP4)

Chemical synthesis, photocharacterization, biological data, protein crystallization, and NMR spectra (PDF)

■ AUTHOR INFORMATION

Corresponding Author

Oliver Thorn-Seshold − *Department of Pharmacy, Ludwig-Maximilians University of Munich, Munich 81377, Germany;* orcid.org/0000-0003-3981-651X; Email: oliver.thorn-seshold@cup.lmu.de

Authors

Li Gao − *Department of Pharmacy, Ludwig-Maximilians University of Munich, Munich 81377, Germany*

Joyce C. M. Meiring − *Cell Biology, Neurobiology and Biophysics, Department of Biology, Faculty of Science, Utrecht University, Utrecht CH 3584, Netherlands*

Adam Varady − *St. Anna Children's Cancer Research Institute (CCRI), Vienna 1090, Austria*

Iris E. Ruider − *Physics Department and Center for Protein Assemblies CPA, Technical University of Munich, Garching 85747, Germany*

Constanze Heise − *Department of Pharmacy, Ludwig-Maximilians University of Munich, Munich 81377, Germany*

Maximilian Wranik − *Laboratory of Biomolecular Research, Division of Biology and Chemistry, Paul Scherrer Institut, Villigen 5232, Switzerland*

Cecilia D. Velasco − *Laboratory of Neurobiology, Department of Pathology and Experimental Therapy, Institute of Neurosciences, University of Barcelona, Barcelona 08907, Spain; Bellvitge Biomedical Research Institute (IDIBELL), Barcelona 08907, Spain;* orcid.org/0000-0003-1527-607X

Jennifer A. Taylor − *Department of Biology, University of Washington, Seattle, Washington 98195, United States*

Beatrice Terni − *Laboratory of Neurobiology, Department of Pathology and Experimental Therapy, Institute of Neurosciences, University of Barcelona, Barcelona 08907, Spain; Bellvitge Biomedical Research Institute (IDIBELL), Barcelona 08907, Spain*

Tobias Weinert − *Laboratory of Biomolecular Research, Division of Biology and Chemistry, Paul Scherrer Institut, Villigen 5232, Switzerland*

Jörg Standfuss − *Laboratory of Biomolecular Research, Division of Biology and Chemistry, Paul Scherrer Institut, Villigen 5232, Switzerland*

Clemens C. Cabernard − *Department of Biology, University of Washington, Seattle, Washington 98195, United States*

Artur Llobet − *Laboratory of Neurobiology, Department of Pathology and Experimental Therapy, Institute of Neurosciences, University of Barcelona, Barcelona 08907, Spain; Bellvitge Biomedical Research Institute (IDIBELL), Barcelona 08907, Spain*

Michel O. Steinmetz − *Laboratory of Biomolecular Research, Division of Biology and Chemistry, Paul Scherrer Institut, Villigen 5232, Switzerland; Biozentrum, University of Basel, Basel 4056, Switzerland;* orcid.org/0000-0001-6157-3687

Andreas R. Bausch − *Physics Department and Center for Protein Assemblies CPA, Technical University of Munich, Garching 85747, Germany*

Martin Distel − *St. Anna Children's Cancer Research Institute (CCRI), Vienna 1090, Austria; Zebrafish Platform Austria for Preclinical Drug Screening (ZANDR), Vienna 1090, Austria*

Julia Thorn-Seshold − *Department of Pharmacy, Ludwig-Maximilians University of Munich, Munich 81377, Germany;* orcid.org/0000-0002-4879-4159

Anna Akhmanova − *Cell Biology, Neurobiology and Biophysics, Department of Biology, Faculty of Science, Utrecht University, Utrecht CH 3584, Netherlands*

Complete contact information is available at: https://pubs.acs.org/10.1021/jacs.2c01020

Funding

This research was supported by funds from the German Research Foundation (DFG: Emmy Noether grant number 400324123 to O.T.-S.; SFB 1032 number 201269156 project B09 to O.T.-S. and project A10 to A.R.B.; SFB TRR 152 number 239283807 project P24 to O.T.-S.; and SPP 1926 number 426018126 project XVIII to O.T.-S.). J.C.M.M. acknowledges support from an EMBO Long Term Fellowship (ALTF 261-2019). A.V. acknowledges support by a DOC fellowship of the Austrain Academy of Sciences (ÖAW). J.T.-S. acknowledges support from a Joachim Herz Foundation Stipend. A.R.B. gratefully acknowledges the financial support of the European Research Council (ERC) through the funding of the grant Principles of Integrin Mechanics and Adhesion (PoINT). A.L. acknowledges funding from the Spanish government (Ministerio de Ciencia e Innovación), grant RTI2018-096948-B-100 (A.L.), co-funded by the European Regional Development Fund (ERDF). M.D. acknowledges funding from the Austrian Research Promotion Agency (FFG) project 7940628 (Danio4Can). C.C.C. is supported by NIH grant 1R01GM126029.

Notes

The authors declare no competing financial interest.

■ ACKNOWLEDGMENTS

We are grateful to Henrietta Lacks, now deceased, and to her surviving family members for their contributions to biomedical research. We thank Monique Preusse for early cell viability testing, and Rebekkah Hammar for performing the tubulin polymerization assay. We thank Christian Gabka from the Nymphenburg Clinic for Plastic and Aesthetic Surgery, Munich 80637, Germany, for providing primary human mammary gland tissue.

■ REFERENCES

(1) Stepanova, T.; Slemmer, J.; Hoogenraad, C. C.; Lansbergen, G.; Dortland, B.; De Zeeuw, C. I.; Grosveld, F.; van Cappellen, G.; Akhmanova, A.; Galjart, N. Visualization of Microtubule Growth in Cultured Neurons via the Use of EB3-GFP (End-Binding Protein 3-Green Fluorescent Protein). *J. Neurosci.* **2003**, *23*, 2655−2664.

(2) Kleele, T.; Marinković, P.; Williams, P. R.; Stern, S.; Weigand, E. E.; Engerer, P.; Naumann, R.; Hartmann, J.; Karl, R. M.; Bradke, F.; Bishop, D.; Herms, J.; Konnerth, A.; Kerschensteiner, M.; Godinho, L.; Misgeld, T. An Assay to Image Neuronal Microtubule Dynamics in Mice. *Nat. Commun.* **2014**, *5*, No. 4827.

(3) Goglia, A. G.; Toettcher, J. E. A Bright Future: Optogenetics to Dissect the Spatiotemporal Control of Cell Behavior. *Curr. Opin. Chem. Biol.* **2019**, *48*, 106−113.

(4) Hoorens, M. W. H.; Szymanski, W. Reversible, Spatial and Temporal Control over Protein Activity Using Light. *Trends Biochem. Sci.* **2018**, *43*, 567−575.

(5) Borowiak, M.; Nahaboo, W.; Reynders, M.; Nekolla, K.; Jalinot, P.; Hasserodt, J.; Rehberg, M.; Delattre, M.; Zahler, S.; Vollmar, A.; Trauner, D.; Thorn-Seshold, O. Photoswitchable Inhibitors of Microtubule Dynamics Optically Control Mitosis and Cell Death. *Cell* **2015**, *162*, 403−411.

(6) Borowiak, M.; Küllmer, F.; Gegenfurtner, F.; Peil, S.; Nasufovic, V.; Zahler, S.; Thorn-Seshold, O.; Trauner, D.; Arndt, H.-D. Optical Manipulation of F-Actin with Photoswitchable Small Molecules. *J. Am. Chem. Soc.* **2020**, *142*, 9240−9249.

(7) Glotzer, M. The 3Ms of Central Spindle Assembly: Microtubules, Motors and MAPs. *Nat. Rev. Mol. Cell Biol.* **2009**, *10*, 9−20.

(8) Kapitein, L. C.; Hoogenraad, C. C. Building the Neuronal Microtubule Cytoskeleton. *Neuron* **2015**, *87*, 492−506.

(9) van Haren, J.; Charafeddine, R. A.; Ettinger, A.; Wang, H.; Hahn, K. M.; Wittmann, T. Local Control of Intracellular Microtubule Dynamics by EB1 Photodissociation. *Nat. Cell Biol.* **2018**, *20*, 252−261.

(10) Adikes, R. C.; Hallett, R. A.; Saway, B. F.; Kuhlman, B.; Slep, K. C. Control of Microtubule Dynamics Using an Optogenetic Microtubule plus End−F-Actin Cross-Linker. *J. Cell Biol.* **2018**, *217*, 779−793.

(11) Meiring, J. C. M.; Grigoriev, I.; Nijenhuis, W.; Kapitein, L. C.; Akhmanova, A. Opto-Katanin: An Optogenetic Tool for Localized Microtubule Disassembly. *bioRxiv* **2021**, *22*, No. 473806.

(12) Liu, G. Y.; Chen, S.-C.; Shaiv, K.; Hong, S.-R.; Yang, W.-T.; Huang, S.-H.; Chang, Y.-C.; Cheng, H.; Lin, Y.-C. Precise Control of Microtubule Disassembly in Living Cells. *bioRxiv* **2021**, *31*, No. 463668.

(13) Wühr, M.; Tan, E. S.; Parker, S. K.; Detrich, H. W.; Mitchison, T. J. A Model for Cleavage Plane Determination in Early Amphibian and Fish Embryos. *Curr. Biol.* **2010**, *20*, 2040−2045.

(14) Josa-Culleré, L.; Llebaria, A. In the Search for Photocages Cleavable with Visible Light: An Overview of Recent Advances and Chemical Strategies. *ChemPhotoChem* **2021**, *5*, 296−314.

(15) Müller-Deku, A.; Meiring, J. C. M.; Loy, K.; Kraus, Y.; Heise, C.; Bingham, R.; Jansen, K. I.; Qu, X.; Bartolini, F.; Kapitein, L. C.; Akhmanova, A.; Ahlfeld, J.; Trauner, D.; Thorn-Seshold, O. Photoswitchable Paclitaxel-Based Microtubule Stabilisers Allow Optical Control over the Microtubule Cytoskeleton. *Nat. Commun.* **2020**, *11*, No. 4640.

(16) Gao, L.; Meiring, J. C. M.; Heise, C.; Rai, A.; Müller-Deku, A.; Akhmanova, A.; Thorn-Seshold, J.; Thorn-Seshold, O. Photoswitchable Epothilone-Based Microtubule Stabilisers Allow GFP-Imaging-Compatible, Optical Control over the Microtubule Cytoskeleton. *Angew. Chem., Int. Ed.* **2021**, *48*, No. e202114614.

(17) Rastogi, S. K.; Zhao, Z.; Gildner, M. B.; Shoulders, B. A.; Velasquez, T. L.; Blumenthal, M. O.; Wang, L.; Li, X.; Hudnall, T. W.; Betancourt, T.; Du, L.; Brittain, W. J. Synthesis, Optical Properties and in Vitro Cell Viability of Novel Spiropyrans and Their Photostationary States. *Tetrahedron* **2021**, *80*, No. 131854.

(18) Gao, L.; Meiring, J. C. M.; Kraus, Y.; Wranik, M.; Weinert, T.; Pritzl, S. D.; Bingham, R.; Ntouliou, E.; Jansen, K. I.; Olieric, N.; Standfuss, J.; Kapitein, L. C.; Lohmüller, T.; Ahlfeld, J.; Akhmanova, A.; Steinmetz, M. O.; Thorn-Seshold, O. A Robust, GFP-Orthogonal Photoswitchable Inhibitor Scaffold Extends Optical Control over the Microtubule Cytoskeleton. *Cell Chem. Biol.* **2021**, *28*, 228−241.

(19) Sailer, A.; Meiring, J. C. M.; Heise, C.; Pettersson, L. N.; Akhmanova, A.; Thorn-Seshold, J.; Thorn-Seshold, O. Pyrrole Hemithioindigo Antimitotics with Near-Quantitative Bidirectional Photoswitching That Photocontrol Cellular Microtubule Dynamics with Single-Cell Precision. *Angew. Chem., Int. Ed.* **2021**, *60*, 23695−23704.

(20) Sailer, A.; Ermer, F.; Kraus, Y.; Lutter, F. H.; Donau, C.; Bremerich, M.; Ahlfeld, J.; Thorn-Seshold, O. Hemithioindigos for Cellular Photopharmacology: Desymmetrised Molecular Switch Scaffolds Enabling Design Control over the Isomer-Dependency of Potent Antimitotic Bioactivity. *ChemBioChem* **2019**, *20*, 1305−1314.

(21) Sailer, A.; Ermer, F.; Kraus, Y.; Bingham, R.; Lutter, F. H.; Ahlfeld, J.; Thorn-Seshold, O. Potent Hemithioindigo-Based Antimitotics Photocontrol the Microtubule Cytoskeleton in Cellulo. *Beilstein J. Org. Chem.* **2020**, *16*, 125−134.

(22) Engdahl, A. J.; Torres, E. A.; Lock, S. E.; Engdahl, T. B.; Mertz, P. S.; Streu, C. N. Synthesis, Characterization, and Bioactivity of the Photoisomerizable Tubulin Polymerization Inhibitor Azo-Combretastatin A4. *Org. Lett.* **2015**, *17*, 4546−4549.

(23) Zenker, J.; White, M. D.; Gasnier, M.; Alvarez, Y. D.; Lim, H. Y. G.; Bissiere, S.; Biro, M.; Plachta, N. Expanding Actin Rings Zipper the Mouse Embryo for Blastocyst Formation. *Cell* **2018**, *173*, 776−791.

(24) Theisen, U.; Ernst, A. U.; Heyne, R. L. S.; Ring, T. P.; Thorn-Seshold, O.; Köster, R. W. Microtubules and Motor Proteins Support Zebrafish Neuronal Migration by Directing Cargo. *J. Cell Biol.* **2020**, *219*, No. e201908040.
(25) Gavin, J.; Ruiz, J. F. M.; Kedziora, K.; Windle, H.; Kelleher, D. P.; Gilmer, J. F. Structure Requirements for Anaerobe Processing of Azo Compounds: Implications for Prodrug Design. *Bioorg. Med. Chem. Lett.* **2012**, *22*, 7647−7652.
(26) Sheldon, J. E.; Dcona, M. M.; Lyons, C. E.; Hackett, J. C.; Hartman, M. C. T. Photoswitchable Anticancer Activity via Trans-Cis Isomerization of a Combretastatin A-4 Analog. *Org. Biomol. Chem.* **2016**, *14*, 40−49.
(27) An, Y.; Chen, C.; Zhu, J.; Dwivedi, P.; Zhao, Y.; Wang, Z. Hypoxia-Induced Activity Loss of a Photo-Responsive Microtubule Inhibitor Azobenzene Combretastatin A4. *Front. Chem. Sci. Eng.* **2020**, *14*, 880−888.
(28) Hüll, K.; Morstein, J.; Trauner, D. In Vivo Photopharmacology. *Chem. Rev.* **2018**, *118*, 10710−10747.
(29) Lachmann, D.; Lahmy, R.; König, B. Fulgimides as Light-Activated Tools in Biological Investigations: Fulgimides as Light-Activated Tools in Biological Investigations. *Eur. J. Org. Chem.* **2019**, *2019*, 5018−5024.
(30) Fuchter, M. J. On the Promise of Photopharmacology Using Photoswitches: A Medicinal Chemist's Perspective. *J. Med. Chem.* **2020**, *63*, 11436−11447.
(31) Welleman, I. M.; Hoorens, M. W. H.; Feringa, B. L.; Boersma, H. H.; Szymański, W. Photoresponsive Molecular Tools for Emerging Applications of Light in Medicine. *Chem. Sci.* **2020**, *11*, 11672−11691.
(32) Gaspari, R.; Prota, A. E.; Bargsten, K.; Cavalli, A.; Steinmetz, M. O. Structural Basis of Cis- and Trans-Combretastatin Binding to Tubulin. *Chem* **2017**, *2*, 102−113.
(33) Tarade, D.; Ma, D.; Pignanelli, C.; Mansour, F.; Simard, D.; Berg, S.; van den Gauld, J.; McNulty, J.; Pandey, S. Structurally Simplified Biphenyl Combretastatin A4 Derivatives Retain in Vitro Anti-Cancer Activity Dependent on Mitotic Arrest. *PLoS One* **2017**, *12*, No. e0171806.
(34) Jacobson, P. Ueber Bildung von Anhydroverbindungen Des Orthoamidophenylmercaptans Aus Thioaniliden. *Ber. Dtsch. Chem. Ges.* **1886**, *19*, 1067−1077.
(35) Ma, D.; Xie, S.; Xue, P.; Zhang, X.; Dong, J.; Jiang, Y. Efficient and Economical Access to Substituted Benzothiazoles: Copper-Catalyzed Coupling of 2-Haloanilides with Metal Sulfides and Subsequent Condensation. *Angew. Chem., Int. Ed.* **2009**, *48*, 4222−4225.
(36) Tron, G. C.; Pirali, T.; Sorba, G.; Pagliai, F.; Busacca, S.; Genazzani, A. A. Medicinal Chemistry of Combretastatin A4: Present and Future Directions. *J. Med. Chem.* **2006**, *49*, 3033−3044.
(37) Kraus, Y.; Glas, C.; Melzer, B.; Gao, L.; Heise, C.; Preuße, M.; Ahlfeld, J.; Bracher, F.; Thorn-Seshold, O. Isoquinoline-Based Biaryls as a Robust Scaffold for Microtubule Inhibitors. *Eur. J. Med. Chem.* **2020**, *186*, No. 111865.
(38) Thorn-Seshold, O.; Meiring, J. C. M. Photocontrolling Microtubule Dynamics with Photoswitchable Chemical Reagents. In *Microtubules—Methods and Protocols*; Springer International Publishing, 2022; Chapter 26.
(39) Florian, S.; Mitchison, T. J. Anti-Microtubule Drugs. In *The Mitotic Spindle: Methods and Protocols*; Chang, P.; Ohi, R., Eds.; Springer: New York, NY, 2016; Vol. *1413*, pp 403−421.
(40) Roostalu, J.; Thomas, C.; Cade, N. I.; Kunzelmann, S.; Taylor, I. A.; Surrey, T. The Speed of GTP Hydrolysis Determines GTP Cap Size and Controls Microtubule Stability. *eLife* **2020**, *9*, No. e51992.
(41) Linnemann, J. R.; Miura, H.; Meixner, L. K.; Irmler, M.; Kloos, U. J.; Hirschi, B.; Bartsch, H. S.; Sass, S.; Beckers, J.; Theis, F. J.; Gabka, C.; Sotlar, K.; Scheel, C. H. Quantification of Regenerative Potential in Primary Human Mammary Epithelial Cells. *Development* **2015**, *31*, 3239−3251.
(42) Buchmann, B.; Engelbrecht, L. K.; Fernandez, P.; Hutterer, F. P.; Raich, M. K.; Scheel, C. H.; Bausch, A. R. Mechanical Plasticity of Collagen Directs Branch Elongation in Human Mammary Gland Organoids. *Nat. Commun.* **2021**, *12*, No. 2759.
(43) Hofer, M.; Lutolf, M. P. Engineering Organoids. *Nat. Rev. Mater.* **2021**, *6*, 402−420.
(44) Kopf, A.; Renkawitz, J.; Hauschild, R.; Girkontaite, I.; Tedford, K.; Merrin, J.; Thorn-Seshold, O.; Trauner, D.; Häcker, H.; Fischer, K.-D.; Kiermaier, E.; Sixt, M. Microtubules Control Cellular Shape and Coherence in Amoeboid Migrating Cells. *J. Cell Biol.* **2020**, *219*, No. e201907154.
(45) Vandestadt, C.; Vanwalleghem, G. C.; Castillo, H. A.; Li, M.; Schulze, K.; Khabooshan, M.; Don, E.; Anko, M.-L.; Scott, E. K.; Kaslin, J. Early Migration of Precursor Neurons Initiates Cellular and Functional Regeneration after Spinal Cord Injury in Zebrafish. *bioRxiv* **2019**, No. 539940.
(46) Cabernard, C.; Doe, C. Q. Apical/Basal Spindle Orientation Is Required for Neuroblast Homeostasis and Neuronal Differentiation in Drosophila. *Dev. Cell* **2009**, *17*, 134−141.
(47) Karpova, N.; Bobinnec, Y.; Fouix, S.; Huitorel, P.; Debec, A. Jupiter, a New Drosophila Protein Associated with Microtubules. *Cell Motil.* **2006**, *63*, 301−312.
(48) Royou, A.; Sullivan, W.; Karess, R. Cortical Recruitment of Nonmuscle Myosin II in Early Syncytial Drosophila Embryos: Its Role in Nuclear Axial Expansion and Its Regulation by Cdc2 Activity. *J. Cell Biol.* **2002**, *158*, 127−137.
(49) Rusan, N. M.; Peifer, M. A Role for a Novel Centrosome Cycle in Asymmetric Cell Division. *J. Cell Biol.* **2007**, *177*, 13−20.
(50) Cabernard, C.; Prehoda, K. E.; Doe, C. Q. A Spindle-Independent Cleavage Furrow Positioning Pathway. *Nature* **2010**, *467*, 91−94.
(51) Connell, M.; Cabernard, C.; Ricketson, D.; Doe, C. Q.; Prehoda, K. E. Asymmetric Cortical Extension Shifts Cleavage Furrow Position in Drosophila Neuroblasts. *Mol. Biol. Cell* **2011**, *22*, 4220−4226.
(52) Roberts, A.; Borisyuk, R.; Buhl, E.; Ferrario, A.; Koutsikou, S.; Li, W.-C.; Soffe, S. R. The Decision to Move: Response Times, Neuronal Circuits and Sensory Memory in a Simple Vertebrate. *Proc. R. Soc. B* **2019**, *286*, No. 20190297.
(53) Distel, M.; Hocking, J. C.; Volkmann, K.; Köster, R. W. The Centrosome Neither Persistently Leads Migration nor Determines the Site of Axonogenesis in Migrating Neurons in Vivo. *J. Cell Biol.* **2010**, *191*, 875−890.
(54) Distel, M.; Wullimann, M. F.; Köster, R. W. Optimized Gal4 Genetics for Permanent Gene Expression Mapping in Zebrafish. *Proc. Natl. Acad. Sci. U.S.A.* **2009**, *106*, 13365−13370.
(55) Fortin, D. L.; Banghart, M. R.; Dunn, T. W.; Borges, K.; Wagenaar, D. A.; Gaudry, Q.; Karakossian, M. H.; Otis, T. S.; Kristan, W. B.; Trauner, D.; Kramer, R. H. Photochemical Control of Endogenous Ion Channels and Cellular Excitability. *Nat. Methods* **2008**, *5*, 331−338.
(56) Laprell, L.; Tochitsky, I.; Kaur, K.; Manookin, M. B.; Stein, M.; Barber, D. M.; Schön, C.; Michalakis, S.; Biel, M.; Kramer, R. H.; Sumser, M. P.; Trauner, D.; Gelder, R. N. V. Photopharmacological Control of Bipolar Cells Restores Visual Function in Blind Mice. *J. Clin. Invest.* **2017**, *127*, 2598−2611.
(57) Matera, C.; Gomila, A. M. J.; Camarero, N.; Libergoli, M.; Soler, C.; Gorostiza, P. Photoswitchable Antimetabolite for Targeted Photoactivated Chemotherapy. *J. Am. Chem. Soc.* **2018**, *140*, 15764−15773.
(58) Babii, O.; Afonin, S.; Schober, T.; Garmanchuk, L. V.; Ostapchenko, L. I.; Yurchenko, V.; Zozulya, S.; Tarasov, O.; Pishel, I.; Ulrich, A. S.; Komarov, I. V. Peptide Drugs for Photopharmacology: How Much of a Safety Advantage Can Be Gained by Photocontrol? *Future Drug Discovery* **2020**, *2*, No. FDD28.
(59) Afonin, S.; Babii, O.; Reuter, A.; Middel, V.; Takamiya, M.; Strähle, U.; Komarov, I. V.; Ulrich, A. S. Light-Controllable Dithienylethene-Modified Cyclic Peptides: Photoswitching the in Vivo Toxicity in Zebrafish Embryos. *Beilstein J. Org. Chem.* **2020**, *16*, 39−49.

https://doi.org/10.1021/jacs.2c01020
J. Am. Chem. Soc. 2022, 144, 5614−5628